Reprinted from
Journal of Imaging Science and Technology® 62(4): 040407-1–040407-12, 2018.

Process Development of Large Area R2R Printing and Sintering of Conductive Patterns by Inkjet and Infra-Red Technologies Tailored for Printed Electronics

Kalyan Yoti Mitra
Fraunhofer Institute for Electronic Nano Systems ENAS, Department of Printed Functionalities, 09126 Chemnitz, Germany
E-mail: kalyanyoti.mitra@enas.fraunhofer.de

Sunil Kapadia, Melinda Hartwig▲, and Enrico Sowade
Technische Universität Chemnitz, Department of Digital Printing and Imaging Technology, 09126 Chemnitz, Germany

Zhenxing Xu
PadaLuma Ink-Jet-Solutions GmbH & Co. KG (Palis), 91459 Markt Erlbach, Germany

Reinhard R. Baumann▲
Fraunhofer Institute for Electronic Nano Systems ENAS, Department of Printed Functionalities, 09126 Chemnitz, Germany
Technische Universität Chemnitz, Department of Digital Printing and Imaging Technology, 09126 Chemnitz, Germany

Ralf Zichner
Fraunhofer Institute for Electronic Nano Systems ENAS, Department of Printed Functionalities, 09126 Chemnitz, Germany

Abstract. *The technological advancement in the field of printed electronics over roll-to-roll (R2R) platform has become very attractive, because of the several advantages such as mass production, large area application, cost-saving and high-speed capabilities. The inkjet technology, on the other hand, among other printing technologies promotes individualization and contact-less deposition process qualities. In this article, the authors demonstrate the state of the art R2R setup for printing silver (Ag) conductive patterns on PEN substrate using inkjet and infra-red technologies. The deposition of the conductive patterns was accomplished using a nanoparticle-based Ag ink and industrial printheads from Fujifilm Dimatix. The novelty of the research work is realization of a print setup, consisting of an industry relevant flexible printhead assembly and drop evaluation station, which are mounted over a R2R printing system. The entire setup allows the user to first evaluate the ejection of the droplets and then stabilize the print parameters without involving the web substrate, followed by re-positioning of the inkjet assembly back to the R2R printing system. The capability of the print setup is exhibited by varying the printing resolution for the defined digital patterns. In addition, the post-treatment of the conductive patterns was tailored with the implementation of an infra-red based sintering module from Heraeus Noblelight GmbH. The power density of the filaments from the sintering module was varied to achieve the maximum conductivity and to ensure no physical damage to the patterns and substrate. The results indicate that such a print setup is very flexible and can offer several benefits to the printing process of conductive patterns, e.g., obtaining line width below 80 μm and sheet resistance of about 0.5 Ω/□, with the advantage of sintering the patterns within 20 s.*
[DOI: 10.2352/J.ImagingSci.Technol.2018.62.4.040407]

▲ IS&T Members.

Received Mar. 1, 2018; accepted for publication May 23, 2018; published online July 30, 2018. Associate Editor: Jihoon Kim.
1062-3701/2018/62(4)/040407/12/$25.00

1. INTRODUCTION

In the last decade, there has been a drastic increase in the interest of printed electronic products. Printed electronics is evolving based on the promise to make electronics available to the market at low cost, that can last for a short life cycle. In this case, the main focus is brought forward to fabricate electronic devices and their corresponding fundamental building blocks. For developing the electronic device layer stacks, a particular process workflow is required. Similar to the workflow of any other graphic arts industry, here also, for the printed electronics, there are in total three process steps: (a) Pre-press (development of patterns/designs and management of digital data), (b) Press (deposition of materials on substrate with required resolution, print definition and dimension etc.) and (c) Post-press (drying, sintering and curing of the deposited material layer) [1, 2]. For the development of printed electronic products, several printing/coating technologies are generally being used due to their technological properties, e.g., gravure printing, screen printing, flexography, slot die coating, spray coating and inkjet printing technology [3–8]. These technologies offer different printing characteristics, e.g., high resolution, thicker layers, smoother layers, high edge sharpness, high scalability and precision in print production, and even digital fabrication of the printed electronic products. The technologies, e.g., gravure, flexography and screen printing technologies are well-known for their R2R print processing capabilities [9, 10]. Although they are high productive printing technologies, they lack in providing solution for "Batch size of One & Turn over time of Zero" — Short Runs, that is especially required in the field of printed electronics. In printed electronics, there is always a requirement to customize and/or modify the design of an electronic component according to the application environment, where there would be scenarios to downscale or reconfigure the architecture of the printed devices. This spontaneous modification in the functional layer with regard to the device can be very inconvenient (especially when the printing is accomplished for minimal iterations), if a non-digital based printing technology is chosen where the patterns are expected to be not flexible fundamentally. This inability to provide direct solutions arrives from the basic technological background, i.e., the involvement of intermediate plates/forms for the printing processes. Besides this, the manufacturing of such plates/forms demand high efforts, costs and inefficient process steps [11]. Hence, there is a requirement of a digital manufacturing technology, e.g., the inkjet printing technology, that has evolved over the last decade dramatically and has proven as a matured technology which finds itself fitting to various printing application areas, e.g., patterns on textiles, wallpapers, posters, flexible plastics for decoration and daily usage. The technology now offers industry relevant printing speeds, resolution, throughput and accuracy of about 300 m/min, 2000 dpi × 2000 dpi, 1000 m^2/h and 5 μm, respectively [12–15]. Following this digital manufacturing route, an intensive research is foreseen toward the development of numerous electronic devices and implementation of a huge variety of functional ink materials and processes. Several publications can be found where Ag nanoparticle inks are printed using inkjet technology to develop electronic devices such as antennas, thin-film transistors, circuits, etc. Here the researchers mostly consider the conventional thermal sintering methodology, where the sintering temperature and time duration is high, e.g., >130 °C and 30 minutes [16–20]. On the other hand, many researchers have also considered alternative industrial relevant sintering technologies to sinter the Ag layers using infra-red (IR), intense pulsed light (IPL), microwave, plasma and laser powered sources to investigate the dependency of the sintering process and their parameters to the electrical property of the sintered layers [21–23]. The research is mostly based on the sheet-to-sheet (S2S) platform to deposit Ag inks and perform the respective sintering investigations. The sheet resistance and time duration of the sintering process is <1 Ω/□ and mins – ms range, respectively. The technologies, e.g., laser, plasma and microwave will take much time to sinter the layers and even demand for high volume of financial involvements and infrastructure. When industrialization and R2R compatibility of a process development is considered, then IPL and IR sintering tools show the highest potential among all, which are demonstrated by numerous publications [24–27]. Here, mostly the layers are first printed and then transferred to R2R platform for the sintering, and furthermore the process is repeated to achieve either single or multilayer stacks. For developing the electronic devices and to validate the process window in an industrial environment, it is very important that we explicitly consider the research work performed based on the process of scaling up the inkjet technology and involve the R2R environment that could be coupled with an industrial relevant sintering/curing technology, e.g., IPL or IR. The publications which has the highest potential to be considered in this regard are Refs. [28–30]. From the publications, it is noted that inkjet technology conceptually and practically can be upscaled and the capability here is demonstrated by usage of the native resolution from the printheads in R2R dynamic format and altering the jetting frequency and web speed. Next to that, the best post-treatment contenders which can support this deposition process and obtain conductive Ag layers are IR and IPL. Among these two technologies, IR technology has higher technological potential to get integrated into a print setup, firstly because of the relatively low financial investments and secondly that IPL is an effective technology (sintering/curing is achieved in ms range) only for the dried layer or for layers that have less solvent content, which is not the case for inkjet technology. Thus, with this article, we would like to extend the mentioned topic by focusing mainly on the establishment of a flexible installation of the industrial equipment and synchronization between them to R2R inkjet printing platform and sintering/curing the Ag ink using IR on a polymeric substrate using the most optimal parameters.

1.1 *Experimental*

1.2 *Inks and Substrate*

In this research, a polyethylene naphthalate (PEN) based film (Teonex® Q65HA) was used to perform all the experiments. It is a both side pre-treated 125 μm thick film from DuPont Teijin Films. A nano-particle based Ag ink, i.e., SilverJet DGP 40LT-15C from Advanced Nano Products Co. Ltd. was used entirely to perform all the tests. The ink contains 35 wt.% of Ag loading having particle size of 60 ± 2 nm in organic solvents/additives and has viscosity and surface tension values of 15 cPs and 37 dyn/cm, respectively, measured at 40 °C.

1.3 *Print Setup*

The entire research work regarding the print step is divided into two stages. Generally, the R2R printing machines offer high print productivity in short time period and the materials are consumed quickly. The inkjet technology on the other hand offers ejection of ink drops in μL – fL volume at the desired locations precisely, without severe wastage. So, before performing the actual print tests on the R2R platform, few basic investigations were conducted on S2S laboratory printer DMP-2831 from FUJIFILM Dimatix and printheads having 16 nozzles and 10 pL drop volume. The main goal is to evaluate the optimal printing parameters, e.g., drop space and line spacing. Here, the R2R printing platform LaborMAN as shown in Figure 1 from manroland was used to perform the R2R printing tests. The combination of different setups including the gravure and inkjet printing processes is possible in this system.

Once the basic investigations are completed using the laboratory inkjet printer, the patterns will then be

Figure 1. Image showing the R2R printing platform LaborMAN from manroland.

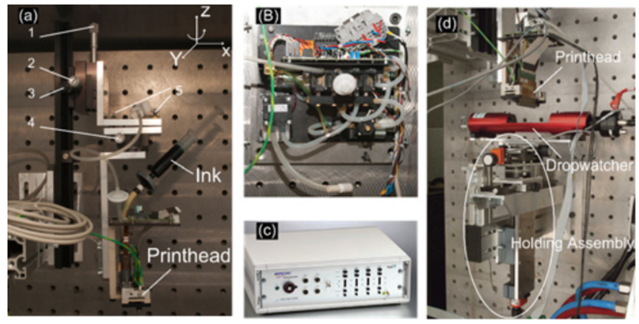

Figure 2. Image showing (a) the inkjet printhead and holding assembly, (b) meniscus pump, (c) Mercury Development Kit [31], and (d) drop watching station.

printed using the R2R inkjet printing system in accordance to the obtained parameters. An industrial inkjet printing module Mercury Development Kit based on the piezoelectric DoD "Versadrop" technology was used, along with an industrially recognized printhead assembly, i.e., Sapphire QS-256/10 AAA printhead from FUJIFILM Dimatix, having 256 nozzles, 10 pL drop volume and a native resolution of 100 dpi [31, 32]. The entire inkjet setup including the inkjet module, drop observation station and an IR drying and sintering module were mounted on the side wall of R2R LaborMAN printing system. The inkjet printhead and holding assembly is shown in Figure 2(a). The holding assembly is realized such that it is restricted to move along X-axis (printing direction). The knobs 1 and 3 are designed for the fine adjustments regarding the movement of the assembly along the Z-axis, whereas the knob 2 is located for the transverse movement of the assembly along the Y-axis. The printhead can be rotated (e.g., addressing different saber angles) by turning knob 4 to achieve the desired printing resolution. A meniscus pump is mounted over the side wall of the R2R printing system to maintain an internal negative pressure inside the printhead, which in return is also connected to the Mercury Development Kit assembly. Such a construction can be seen in Fig. 2(b). The controlling unit of the Mercury Development Kit can be seen in Fig. 2(c). This control unit is connected to the computer, where the Mercury Development Kit software is installed as well as to the printhead. The control unit transmits the digital waveform and heating signals to the printhead, with the parameters that can be controlled over the control unit and software interface [33]. The heating signal is an extra input value which is transferred from the control unit to the printhead, in order to reduce the viscosity of the ink and enable it for the process of drop ejection.

The drop evaluation hardware JetXpert OEM from the company ImageXpert Inc. including a stroboscopic camera, having the possibility to fit different lenses with various magnification was installed [34]. This drop watching station is particularly beneficial for the development of a waveform for a specific printhead and ink, as a pre-make ready step for the inkjet printing process. A digital waveform is set of electronic signals (voltage versus time) that is transferred from the control generator to the piezoelectric actuator at the printhead hardware. These signals create an inverse piezoelectric effect which leads to mechanical deformation, forcing the ink to eject out from the nozzle orifice. These ejected drops from the ink reservoir and printhead are entirely affected by the implemented waveform and its type, which can now be manipulated for further optimization once the drop ejection properties are reviewed using the drop watching station and *in situ* with the application of electronic signals. The drop watching station here has the capability to evaluate the drop volume >1 pL, ejected drop trajectory, drop velocity and distance between the drops. An image of such a construction with a drop watching station is shown in Fig. 2 (d). The drop watching station is positioned just below the printhead assembly and PEN substrate. Just before the printing process, the drop watching station is accessed by sliding out the printhead assembly and aligning it to the drop watching station without disturbing the location of the web. Also, in case of a sudden stop during the printing process, the drop watching station is accessible to re-evaluate the condition of the nozzles and drop ejection.

Equation (1) shows the relationship between the drop velocity (v in m/s), drop ejection/jetting frequency (f in kHz) and printing resolution, i.e., drop space/dot pitch (DS in µm). At higher printing resolution (lower drop space/dot pitch), the jetting frequency should be elevated, or the web speed should be lowered:

$$v = f \cdot DS. \tag{1}$$

Equation (2) describes the function between drop space in Y-axis (Y_{DS}) and θ_k. The direction of the nozzle plate and web forms the angle θ_k. When θ_k is 90°, the nozzle plate and web direction are perpendicular to each other and the printing resolution is 100 dpi ($DS = 254$ µm), which is basically the native resolution of the printhead. The native resolution of a printhead can be defined as the maximum achievable dots per inch (dpi) when the printhead is aligned in a single row and perpendicular to the print travel direction, wherein the dependence is directly proportional to the distance between the nozzles (nozzle pitch). If θ_k is less than 90°, the distance between the nozzles Y_{DS}/nozzle pitch will theoretically decrease over the Y-axis (lower DS)

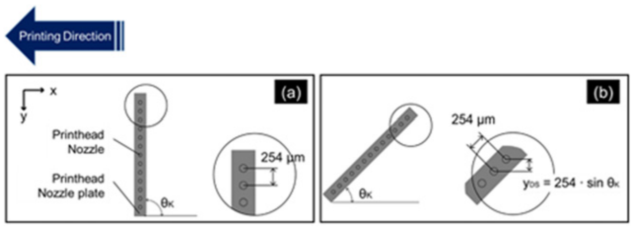

Figure 3. Scheme showing the position of the printhead when (a) perpendicular to the print direction, and when (b) set at an angle to the print direction.

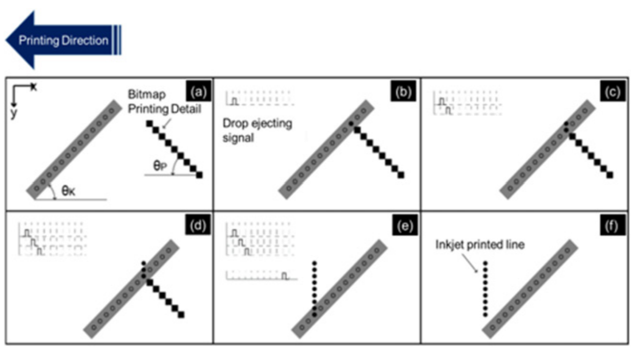

Figure 4. Scheme showing (a) printhead and digital bitmap angled at defined degrees, (b) signal provided to the printhead for the first drop ejection, (c) signal provided to the printhead for the second drop ejection, (d) signal provided to the printhead for the third drop ejection, (e) signal provided to the printhead for the last drop ejection and (f) one row of drops at an angle forming a line perpendicular to the printing direction.

and hence the printing resolution could be increased. Also, it is valid, that in such a situation the printing width for a single pass process step decreases. This is the disadvantage of using such a printing step, but this challenge could be overcome by stitching/stacking several printheads in the orientation of θ_k:

$$Y_{\mathrm{DS}} = 254 \cdot \mathrm{Sin}(\theta_k). \tag{2}$$

The scheme in Figure 3(a) shows the position of the printhead when θ_k is placed at 90°, where the nozzle plate and web travel is perpendicular to each other. In this case the resolution across the printing direction is set to 100 dpi. Using this mentioned resolution, the drops may not fuse with each other (in Y-axis) and printing of line patterns is not feasible. To address this challenge, the printhead needs to be angled to different degrees to achieve specific printing resolution. As depicted in Fig. 3(b), if θ_k is turned to less than 90°, the distance between two nozzles Y_{DS}/nozzle pitch decreases over the Y-axis yielding to a lower drop space/dot pitch and hence the printing resolution is increased. Equation (2) describes the relation between Y_{DS}/nozzle pitch and θ_k. In addition, according to the alignment of the printhead, the digital printing pattern must also be adjusted. A scheme is shown in Figure 4(a), where the printing pattern and printhead are angled at opposite geometrical orientations. The printing process along with the

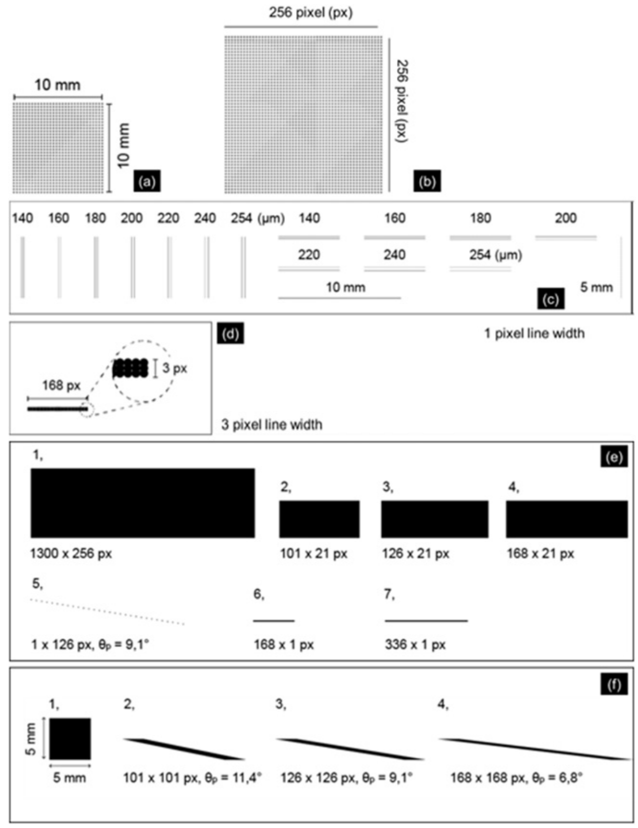

Figure 5. Scheme constituting of printable digital patterns: (a) square pattern containing single dot pixel for DMP-2831, (b) square pattern containing pixel for R2R inkjet system, (c) single pixel lines and (d) triple pixel line patterns of different dimensions printable by DMP-2831, (e) line patterns of different dimensions printable by R2R inkjet system, (f)–1 square pattern printable by DMP-2831 and (f)–2, 3 & 4 R2R inkjet system.

deposition of the individual drops is schematically shown in Fig. 4(b)–(f). Here, the second image shows that the first drop corresponding to the first pixel printed as the web continues to move forward, followed by the printing of the second drop for the second neighboring pixel and so on, until the last drop or pixel is printed. As a result, on the X-axis theoretically all the printed drops will be aligned in a series and perpendicular to the direction of the printing or web travel. Therefore, the drop space Y_{DS}/nozzle pitch is totally dependent upon the θ_k. If the θ_k is set low, then the resulting drop space Y_{DS}/nozzle pitch is also low and vice versa, and thus the digital print pattern must be adjusted accordingly to achieve the desired print resolution.

Figure 5(a) and (b) shows the digital images containing the dot pattern with drop space/dot pitch of 254 µm, i.e., 100 dpi, for DMP-2831 and R2R inkjet printing system. In Fig. 5(c), the line pattern for the DMP-2831 is illustrated. Seven parallel lines are placed horizontally and vertically with length of 5 mm and a gap (nozzle pitch) of 140 µm, 160 µm, 180 µm, 200 µm, 220 µm, 240 µm and 254 µm. These patterns were always printed with drop space/dot pitch of 30 µm, 40 µm and 50 µm, respectively. All these lines are designed with 1 pixel line width and in contrast

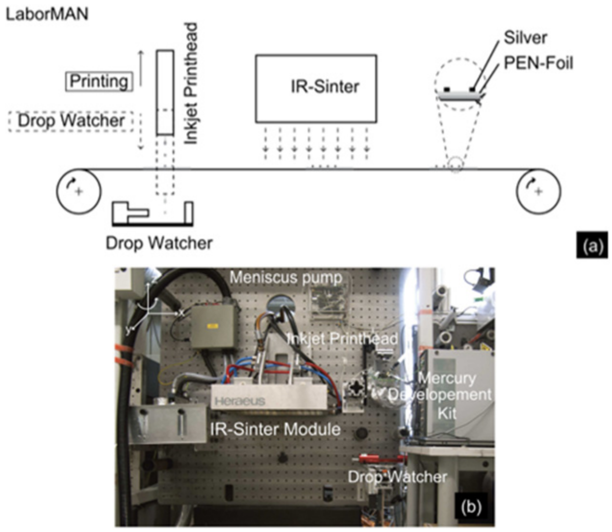

Figure 6. Scheme showing the workflow of (a) drop watching, inkjet printing and sintering of Ag ink at R2R LaborMAN printing system, and (b) image showing the actual printing and sintering setup including every individual components.

Fig. 5(d) shows the line width of 3 pixels and a length of 168 pixels. Fig. 5(e) shows different patterns designed for the print tests at the R2R inkjet printing system. The first pattern has 1300 pixels along the printing direction and 256 pixels across the printing direction. The 2nd, 3rd and 4th pattern belong to a single group and they look identical. These patterns were printed to evaluate the effect of the print quality on the varying deposition parameters, e.g., drop space/dot pitch, web speed, jetting frequency. The 6th and 7th pattern have 168 pixels and 336 pixels length and 1 pixel width. In Fig. 5(f), the 1st pattern was designed for printing squares using DMP-2831. The 2nd, 3rd and 4th patterns from Fig. 5(f) were designed to print the squares but using R2R inkjet printing system and they correspond to the drop space/dot pitch (digital resolution) of 50 μm (508 dpi), 40 μm (635 dpi) and 30 μm (847 dpi), respectively. In total seven experiments were executed using the R2R inkjet printing system. Here, several tasks were approached by varying different patterns, printing and post-treatment parameters. All the parameters are listed in Tables I and II. In Table II, it is demonstrated how a defined printing resolution could be obtained for a certain individual patterns, i.e., by the matching of jetting frequency, web speed and angle of rotation for the printhead.

A schematic representation of the experimental setup for R2R print trials is shown in Figure 6(a), whereas an actual laboratory setup is depicted in Fig. 6(b). A typical sequence of an experiment is as follows: At first the appropriate digital patterns are designed including θ_p and then the patterns (bitmap file) are imported to the GIS software at Mercury Development Kit interface. The printhead angle θ_k and the web speed would be set in the LaborMAN software. This was followed up by setting the jetting frequency again in the GIS software. The PEN film would then be web fed to the R2R printing system and after this preliminary setup the inkjet printing trials were performed.

Table I. Different print trials and parameters.

Trial	Pattern	Web Speed (m/s)	θ_k (deg)	Drop Space (μm)
1	→ Dot pattern & (sinter—hotplate)			
	Fig. 5(b)	0.025	0	254
2	→ Parallel lines with nozzle pitch/distance of (254, 220, 180) μm (sinter—hotplate)			
	Fig. 5(e) - 1	0.025	90, 60, 45.1	30, 40 & 50
3	→ Printing with various web speeds (sinter—hotplate)			
	Fig. 5(e) - 2, 3 & 4	0.025, 0.05, 0.075, 0.1	90	30, 40 & 50
4	→ Printing Lines across printing direction (sinter—hotplate)			
	Fig. 5(e) - 5	0.025	9.1	40
5	→ Printing squares at various drop spaces/dot pitch (sinter—hotplate)			
	Fig. 5(f) - 2, 3 & 4	0.025	6.8, 9.1 & 11.4	30, 40 & 50
6	→ Printing Lines (sinter—IR)			
	Fig. 5(e) - 6 & 7	0.025	90	30
7	→ Printing Squares (sinter—IR)			
	Fig. 5(f) - 4	0.025	6.8	30

Table II. Showing the relationship between drop space, web speed and drop ejection frequency.

Web speed (m/s)	Jetting Frequency (kHz)	Drop Space (μm)
0.025	0.833	30
0.05	1.666	
0.075	2.5	
0.1	3.333	
0.025	0.625	40
0.05	1.25	
0.075	1.875	
0.1	2.5	
0.025	0.5	50
0.05	1	
0.075	1.5	
0.1	2	

1.4 *Sintering*

Once the process of printing is accomplished, the printed layers as comparison are sintered either thermally using hotplate or by IR module. While using a hotplate, the sintering temperature and time durations was fixed at 120 °C for 20 minutes. Figure 7(a) and (b) shows the implemented IR module from Heraeus Noblelight GmbH (wavelength 0.94–1.2 μm) and (c) controlling unit for powering the IR module, which is integrated into LaborMAN R2R printing setup. The IR module has 12 emitter filaments and when all the filaments are switched ON, the power irradiation is distributed uniformly over the entire substrate area. Alternatively, with the help of the equipment's controlling unit, i.e.,

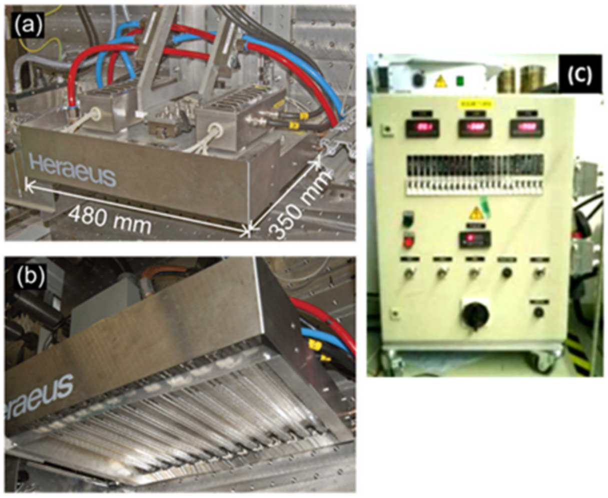

Figure 7. Image showing (a) the IR sintering Module, (b) IR filaments and (c) control unit for powering the integrated R2R module.

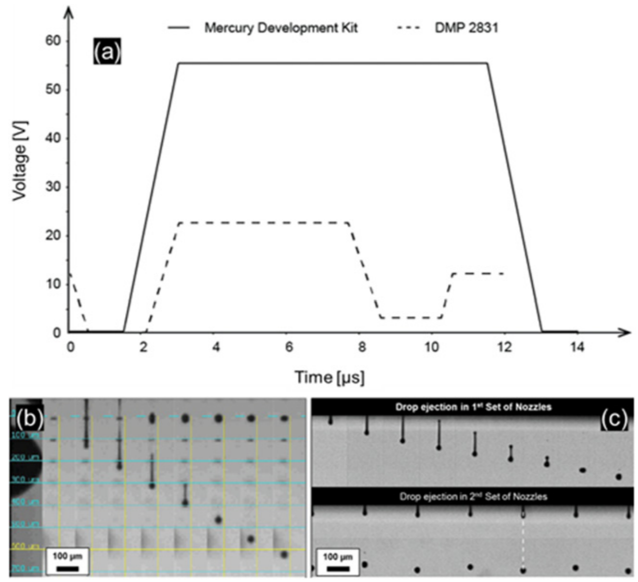

Figure 8. Graph showing (a) the jetting waveform for the Ag ink using 10 pL DMC cartridge fitting to DMP-2831 printer and QS-256/10 AAA class industrial printheads at Mercury Development Kit and image showing drop ejection characteristics for the (b) DMC cartridge and (c) QS class printheads.

shown in Fig. 7(c), the user can also switch ON the filament selectively. This makes the module very compatible with temperature sensitive substrates. For sintering the printed Ag layers using IR module, the supplied electrical power energy density (ED) was set to 1 kW (ED—11.42 J/cm^2), 1.6 kW (ED—18.29 J/cm^2) and 2.5 kW (ED—28.57 J/cm^2). To perform the sintering tests, all IR emitters were illuminated and the distance between the IR module to the substrate for the sintering process was kept constant at 12 cm. The patterns shown in Fig. 5(e) -6 and -7, and (f) - 4 were only sintered using IR module, and in contrast all the other patterns were printed and sintered using hotplate. The printed and sintered layers were then optically evaluated using the Leica DM4000 light microscope. The electrical properties, e.g., sheet and line resistance for all the printed samples were measured using a manual probe system PM5 from Süss Microtec and digital LCR meter.

2. RESULTS AND DISCUSSIONS

2.1 *Deposition analysis*

Figure 8(a) shows the waveforms of the two printing processes. In the DMP-2831, the waveform is indicated with the dashed lines having a pulse width of about 12 μs and an operating maximum voltage of 22.5 V (normalized). The waveform that is indicated with solid line is built for Mercury Development Kit having a pulse width of about 14 μs and a maximum operating voltage of 55 V (normalized). Fig. 8(b) shows the drop formation and ejection trajectory for the two printheads, i.e., DMC cartridge and QS-256/10 AAA class. Both the printheads were well stabilized at similar temperature which is about 40 °C for optimal drop ejection properties. The drop ejection at DMP-2831 is shown in Fig. 8(b), where the image from the ejected drops are captured at every 100 μs strobe delays. The process of drop formation is finished at distance of 600–700 μm from the nozzle plate. The drop velocity was investigated and found to range between 6 and 7 m/s and at low voltage inputs the drop velocity was found to be slower. If the voltage is set higher, the drop velocity increases, but this increase in the velocity limits the drop forming properties, resulting in long tails and/or satellite drops. Therefore, this condition in general was avoided. The measured average drop volume for the DMC cartridge was about 9.8 ± 0.6 pL. The drop formation with the QS-256/10 AAA class printhead in R2R inkjet printing system is shown in Fig. 8(c). Here, both the drop formation as the top image and the working state of different nozzles as bottom image are depicted in the figure. With the help of the drop watching station, measurements were done to evaluate certain parameters from the ejected drops. The results show that the drops have an average volume of about 11 ± 0.8 pL and an average velocity of 3.4 ± 0.3 m/s. From the figure, one can also see that the difference between the velocities among the drops jetting out from a set of nozzles is minimal and they exhibit no satellite formation. In contrast, due to the difference in the architecture and electronic built, e.g., piezoactuator of the printhead, the maximum voltage that is used in the operating waveform for DMC cartridge in DMP-2831 is much lower than the ones from Mercury Development Kit, but the drops on the other hand have a higher speed. For both the printheads, the drop formation quality was found to be stable, flawless and well shaped, which could be ejected reliably for the printing process.

2.2 *Morphological characterization*

The image of the printed dots from using Mercury Development Kit and QS-256/10 AAA class printhead at the R2R printing system can be seen in Figure 9(a)–(c) and using DMP-2831 can be seen in Fig. 9(d). The tests were performed based on the trial 1, mentioned in experimental section.

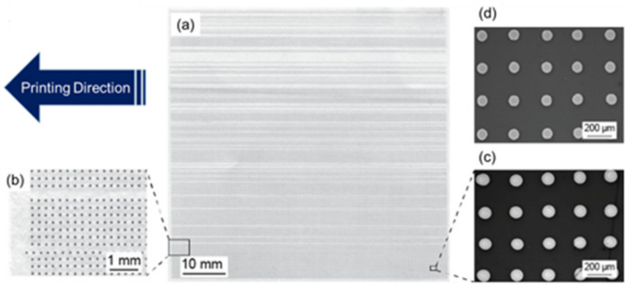

Figure 9. Photo of (a) a printed section containing Ag drops/dots printed at R2R inkjet system using all 256 nozzles from QS-256/10 AAA class printhead and Mercury Development Kit, (b) magnified image from a section where the Ag drops were printed, microscopic images of the drops printed at (c) the same R2R inkjet system, and in contrast with the ones printed with (d) 10 pL DMC cartridges at DMP-2831.

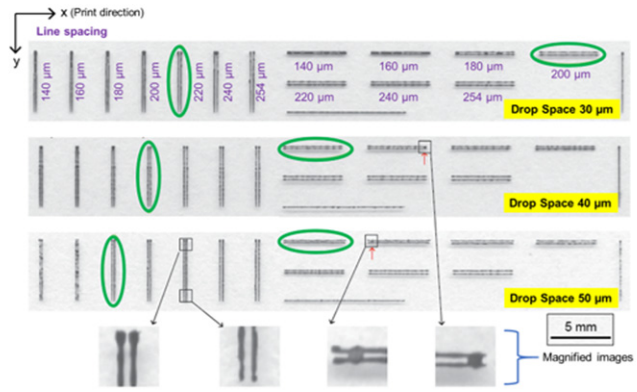

Figure 10. Photos of Ag lines printed with DMC 10 pL printhead and DMP-2831 printer.

Fig. 9(a) gives an overview of the working condition of all the 256 nozzles. Here it can be clearly seen that, along the printing direction all the drops are ejected through same nozzles, and across the printing direction the drops are ejected through different nozzles. In Fig. 9(a) and (b), we can see that at the lower part of the image all the nozzles have been functional, and the top part of the same image shows some of the nozzles are clogged and have not been firing appropriately. Therefore, in this case the printhead is again moved to the drop watching station, where the drop ejection parameters were reviewed and tuned to stabilize the ejection process of the Ag ink from all the nozzles. From the microscopic images shown in Fig. 9(c) and (d), it is concluded that printing of circular dots or drops on top of PEN foil using both the printheads is possible and that they are very comparable. The average diameter of the printed dots in the R2R inkjet printing system was found to be 100 ± 2 μm and the ones printed with DMP-2831 had an average value of 86 ± 1 μm. The dots printed using R2R inkjet printing system has a larger diameter when compared to the dots printed with DMP-2831. The difference in the dot diameter was found to be about 15 μm. The reason behind these relatively larger dots size could be the higher volume of drops ejecting from the nozzles. After purging and tuning the necessary jetting parameters at the Mercury Development Kit, QS-256/10 AAA class printhead and GIS software interface, several nozzles were recovered and now available to show an enhanced operating condition with high stability. Care was always taken to keep the ink in movement all the time during the commencement of the experimental trials.

Figure 10 represents the preliminary results concerning printing of lines on PEN substrate using different drop spaces/dot pitches and geometrical features, using DMP-2831 and DMC cartridges. Along the print direction (X-axis), the lowest designed line spacing was 140 μm (digital). When the printing tests were performed for this line spacing (digital) using the drop space/dot pitch between 30–50 μm, positive results were obtained for the drop space/dot pitch of 40 μm and 50 μm. A clear separation between the printed lines was seen, when both the drop spaces/dot pitches were implemented. In contrast, when drop space/dot pitch of 30 μm was considered, the minimum line spacing required to achieve discrete features was 200 μm. In across the print direction (Y-axis), the lowest line spacing (digital) was 140 μm. It was observed that the characteristic of the printed lines in Y-axis was very different. As shown in Fig. 10, for the lines printed with spacing of 140 μm and 160 μm, there is a high probability that the lines would merge with each other. Here we can see a clear trend that with increasing the printing resolution, there is a definite requirement to implement wider line spacing for obtaining discrete features, e.g., 180 μm spacing for 50 μm drop space/dot pitch, 200 μm spacing for 40 μm drop space/dot pitch and 220 μm spacing for 30 μm drop space/dot pitch. Several tests were conducted to confirm the interpretations and it was finally concluded that the patterns containing line spacing less than 180 μm had no reliability. This was due to the irregular spreading of the ink at different conditions. For this reason, digital line spacing of 254 μm, 220 μm and 180 μm are taken into account and set as the print parameters for the R2R printing system.

Figure 11 represents the microscopic images of the printed lines obtained by varying the drop spaces/dot pitch, line spacings/nozzle pitch and using QS-256/10 AAA class printheads in R2R printing system. The first row from left to right shows the lines printed with 30 μm, 40 μm and 50 μm drop spaces/dot pitches, but with the line spacing of 254 μm. The images positioned in the second and third row from left to right shows the lines printed with 220 μm and 180 μm line spacing/nozzle pitch. The web speed for this specific printing trials was kept constant at 0.025 m/s although the jetting frequency was varied to 0.833 kHz, 0.625 kHz and 0.5 kHz, to achieve the drop space/dot pitch of 30 μm, 40 μm and 50 μm, respectively.

The images in Fig. 11 show that at a line spacing/nozzle pitch of 254 μm and 220 μm results in undisturbed individual line, but at line spacing/nozzle pitch of 180 μm all the lines tend to fuse together irrespective of the used drop space/dot pitch. It could also be concluded that when the lines are printed with 30 μm drop space/dot pitch, the printed features

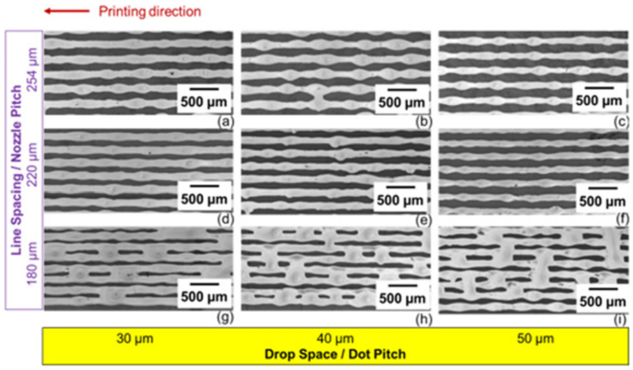

Figure 11. Microscopic images of the printed Ag lines using (a) line and drop spacing of 254 μm and 30 μm; (b) line and drop spacing of 254 μm and 40 μm; (c) line and drop spacing of 254 μm and 50 μm; (d) line and drop spacing of 220 μm and 30 μm; (e) line and drop spacing of 220 μm and 40 μm; (f) line and drop spacing of 220 μm and 50 μm; (g) line and drop spacing of 180 μm and 30 μm; (h) line and drop spacing of 180 μm and 40 μm; and (i) line and drop spacing of 180 μm and 50 μm.

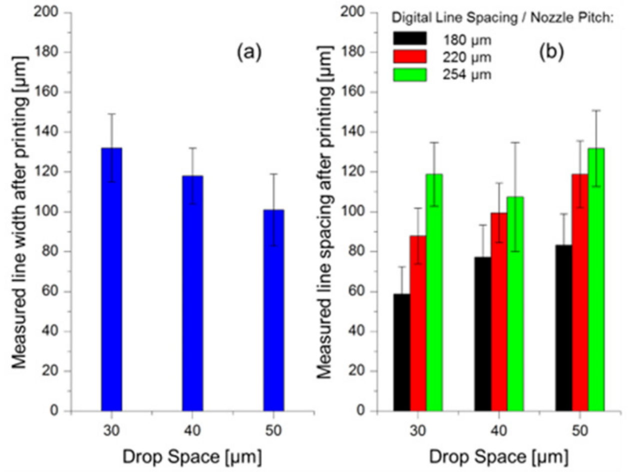

Figure 12. Graph showing the measured (a) single feature line width and (b) line spacing as a function of drop space/dot pitch.

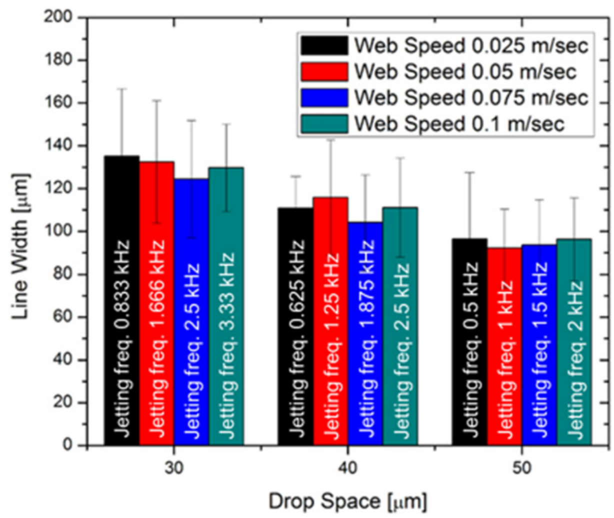

Figure 13. Graph showing the measured line width as function of varying drop space/dot pitch based on different web speeds and jetting frequencies.

suffer from high bulging characteristics. As summary, it is noted that the geometrical parameters, i.e., 220 μm line spacing/nozzle pitch and drop space/dot pitch of 50 μm can be referred as the best parameters, since none of the lines fuses together and they show acceptable feature quality. It is evident from the microscopic images that the printed lines show bulging characteristics due to the unavoidable inconsistent ink/material deposition rate, which was realized here by applying low jetting frequency and web speed. The effective result is demonstrated in Fig. 11. This phenomenon has been explained very clearly in several citations [35–37]. Figure 12 below represents the (a) average line width and (b) line spacing/nozzle pitch as a function of drop space/dot pitch. In Fig. 12(a) and (b) vertical axis shows measured line width and line spacing, blue bar shows the average line width at different drop space/dot pitch on horizontal axis. In Fig. 12(a) the value of 132 ± 17 μm at a drop space/dot pitch of 30 μm was measured as the highest line width. The value of 101 ± 18 μm was measured for the drop space of 50 μm which is the lowest line width and 118 ± 14 μm for 40 μm drop space. In Fig. 12(b) the black, red and green bars in the graph show the average measured values of the different line spacing at different drop spaces/dot pitches. The black bar shows a line spacing/nozzle pitch of 180 μm, where most of the lines are fused together. The red and green bars show also an increasing tendency, i.e., with the increase in the drop space/dot pitch, the printed line spacing is also found to increase. For the un-interrupted lines, the smallest gap at a line spacing/nozzle pitch of 220 μm was found to be 88 ± 14 μm, for drop space/dot pitch of 30 μm. In this graph the standard deviations are usually found to stay between 14 and 19 μm, with an exception shown for the black bar with a drop space/dot pitch of 40 μm, the value is 27 μm. As a conclusion it can be said that, as the drop space/dot pitch is increased the spacing between the printed line increases, because the width of the individual lines reduces. Hence, this correlates the deposition rate of the ink material directly to the printing resolution.

Second part of the trials were performed, by printing the lines with length of 5 mm with different drop spaces by varying the jetting frequency and web speeds simultaneously, as shown in Table II for the R2R inkjet printing system and then sintered on hotplate. After this step, the widths of the printed lines were measured. The results are shown in Figure 13, where the vertical axis shows the measured line widths, whereas the horizontal axis represents the varying drop spaces/dot pitch. Different colored bars show the different printing parameters which is the combination of jetting frequency and web speed, resulting in the same or different drop spaces/dot pitches. In this way, here the R2R inkjet printing system becomes very flexible and versatile in case only one parameter is intended to get changed. The different parameters considered here are corresponding to the values shown in Table II. As conclusion, it can be said that as the printing resolution is decreased or the drop space/dot pitch is increased, the width of the printed line decreases and vice versa. It can also be seen that, for the same drop space there is noticeable difference in the line width, which refers to the printing related tolerances. This tolerance decreases as the printing resolution is decreased, as it is shown for drop space/dot pitch of 50 μm where the average width of the printed line is relatively constant. Finally, it is summarized that the width of the printed lines in R2R printing system is very similar to the results obtained using DMP-2831, e.g., by implementing the optimal parameters and Ag ink, a width of about 100 μm is achievable for printing a single pixel line.

Figure 14(a) shows that three lines are printed along the web direction using R2R inkjet printing system. Line (a-1) and (a-2) were printed using the same parameters (0.025 m/s web speed and 0.5 kHz jetting frequency −50 μm drop space/dot pitch). About 5 minutes after the printing process, they were placed on the hotplate and sintered at 120 °C for 20 minutes. In contrast to this, line (a-3) was printed at 30 μm drop space/dot pitch and immediately sintered in-line with the IR module. The corresponding line widths and standard deviations or tolerances are shown in Fig. 14(a). Most of the lines (seven out of ten printed lines), sintered offline by means of a hotplate gave rise to bulged lines with a tolerance of 18–26 μm. A smooth line feature can be observed in Fig. 14 for line (a-3) with a tolerance of 10 μm. In most of the cases (eight out of ten printed lines), the lines sintered in-line with IR module offered good quality with a low tolerance limit, i.e., below 10 μm. As a conclusion, it can be stated that a homogeneous line shape is achieved when the tolerance in form of standard deviation is below 10 μm. In-line IR sintering/curing could have a positive effect on line quality, due to the low waiting time, uniform radiation coverage and control over the solvent removal from the printed feature. As shown in Fig. 14(b), squares of 5 × 5 mm^2 were printed using R2R inkjet printing system at 30 μm, 40 μm and 50 μm drop spaces. Due to the similar optical appearance, only squares printed at drop space/dot pitch of 40 μm are shown in Fig. 14(b). The patterns were printed several times at the same web speed and altered jetting frequencies. The microscopic images give more details about the edge sharpness of the square printed along the web direction, which looks smoother and across the web direction, looks wavier.

Two lines, i.e., S1 and S2 are shown in Fig. 14(b), all the printed dots on the line S1 come from a nozzle A and on the line S2 the drops come from a nozzle B. The length of S1 is the distance of the first pixel point from the first square and the first pixel point from the second square (the drops come from nozzle A). The length of S2 is the distance from the first pixel point of the first square to the first pixel point of the second square (the drops come from nozzle B). The web speed was kept constant at 0.025 m/s. Since the printhead is oriented obliquely, first comes the drop from

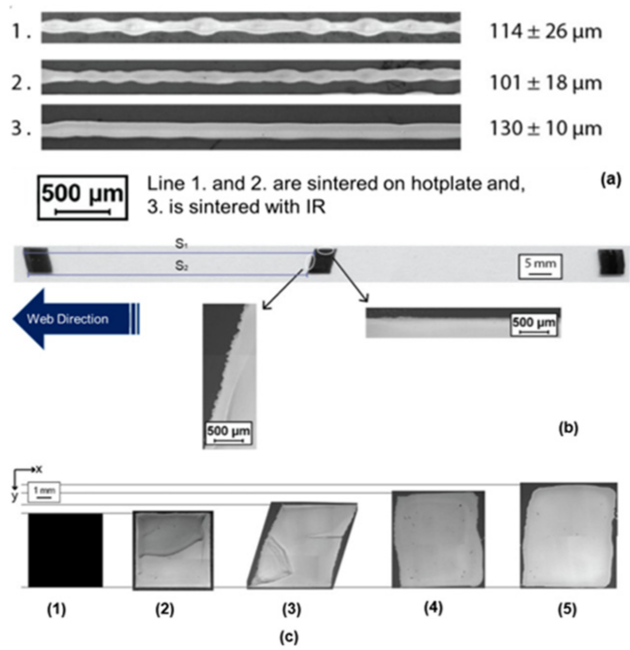

Figure 14. Images showing (a) line morphology, (b) squares printed at 40 μm drop space, (c-1) digital square pattern, (c-2) inkjet printed pattern from DMP-2831, (c-3) inkjet printed patterns from R2R printing system and sintered on hotplate, (c-4) inkjet printed patterns from R2R printing system and sintered by IR at 11.42 J/cm^2, and (c-5) inkjet printed patterns from R2R printing system and sintered using IR at 18.29 J/cm^2.

nozzle A and then comes the drop from nozzle B, assuming the distance of the line is the same. It was recognized that unfortunately the web speed of 0.025 to 0.1 m/s was found to be very slow which caused the maximum instability and that is the reason why lines S1 and S2 had different lengths resulting in irregular shaped squares. Fig. 14(c) shows the result of the squares printed using two printing systems with the same print settings and 30 μm drop space/dot pitch (explained in Table I). Five images are shown with the same magnification and the lower edge was focused in the same line, so that the dimensional difference between the squares is noted. In Fig. 14(c-1), the digital print pattern is shown and in (c-2) the square is printed with DMP-2831 and sintered on a hotplate. After completing the sintering process the printed surface area was optically measured and found to be ∼25 mm^2. In images c-3, c-4 and c-5, the squares are printed using the R2R inkjet printing system, where the only difference is the implemented post-treatment after the print process. In Fig. 14(c-3) the square is sintered on a hotplate, afterward the measured surface area is found to be ∼28 mm^2, i.e., increased by 15%. The fourth and fifth squares were sintered in-line with IR and by different power densities. After the sintering was accomplished, the printed surface was optically measured, and the dimension was found to be 35 and 39 mm^2, which is an increment of 40% and 58%, respectively. As a conclusion, it can be said that process of IR curing increases the temperature within the layer, and reduces the surface energy of the ink, resulting in higher spreading behaviors. The higher is the ED of the sintering process, larger is the expected surface area of the printed pattern. It is speculated that the difference in the heat transfer mechanism from the source to the printed layer in a conventional (bottom to top) and IR (top to bottom) based curing process can be the only reason why the ink spreading is much more controlled but intensified in case of IR curing methodology than the former.

2.3 *Electrical characterization*

Figure 15(a) shows the relationship between the line resistance of the different dimensions and sintering EDs of the IR module. The printed lines had width of ∼130 μm, as they were printed with 30 μm drop space/dot pitch (up to 0.1 m/s web speed and 3.33 kHz jetting frequency). The highest line resistance was found at 11.42 J/cm^2 ED, with the values of 99 ± 10 Ω for the length of 5 mm and 170 ± 9 Ω for the length of 10 mm. The tendency shows that the resistance is decreased as the ED of the IR is increased, but the values for the same lengths to a ED of 18.29 J/cm^2 and 28.57 J/cm^2, respectively, do not make a significant difference. Fig. 15(b) shows the dependence of the measured sheet resistance in Ω/□ to the sintering ED for IR module and constant layer thickness using 30 μm drop space/dot pitch. At ED of 28.57 J/cm^2, the lowest sheet resistance of 0.3 ± 0.04 Ω/□ was obtained. In contrast to this, values of 0.54 ± 0.23 Ω/□ and 0.53 ± 0.03 Ω/□ were achieved for ED of 11.42 J/cm^2 and 18.29 J/cm^2. Here, the obtained sheet resistance of 0.5 Ω/□ is calculated to be about 7% of the conductivity of bulk Ag. It can be seen that the difference between the tolerances in the obtained sheet resistance is very high when ED of 11.42 J/cm^2 and 18.29 J/cm^2 are compared, although the average values remain constant. It is worth noticing in Fig. 15(a) that there is no dramatic difference in the line resistance when the sintering ED is 19.28 J/cm^2 or higher, however, there is a significant difference in the sheet resistance shown in Fig. 15(b) between these EDs.

This difference in the electrical properties occur as an impact, when there is a variation in the sintering process toward the printed pattern, which in this case is affected by the individual pattern definition (line or square) and the corresponding morphology/topology obtained after sintering. These physical characteristics directly affect the electrical properties of the printed Ag features. Although here the drying and sintering process is accomplished in the same manner for both the lines and squares, there is high probability that the lines sinter more uniformly compared to the squares under lower ED. At higher ED the line patterns can attain saturated electrical resistance properties much earlier, due to early stage completion of sintering process. Whereas for the squares, there is still a wide scope for reducing the sheet resistance by applying higher EDs (due to late stage completion of sintering process), as the sheet resistance is defined mainly by the surface related microstructure and thickness of the layer.

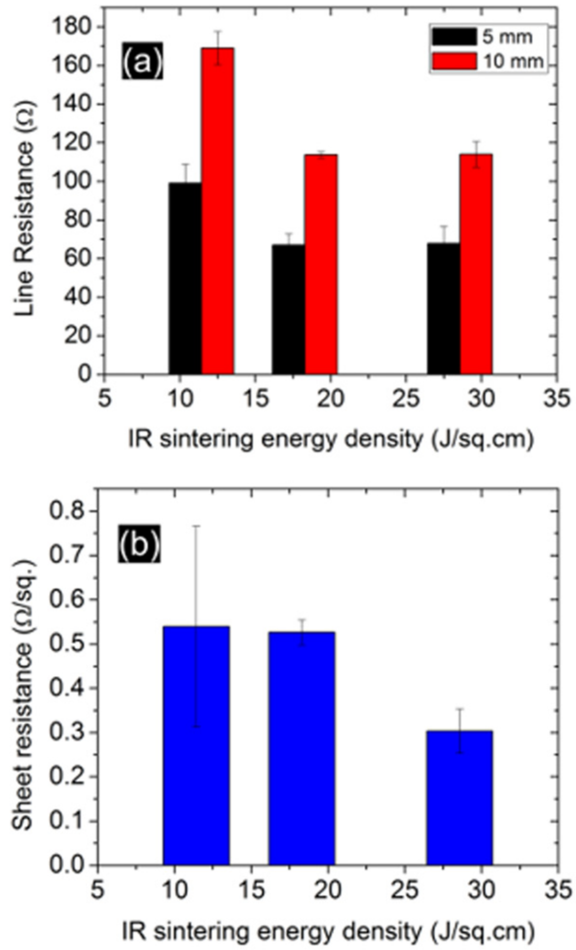

Figure 15. Graph showing (a) line resistance and (b) sheet resistance at different IR power densities.

3. SUMMARY

The entire research work performed here is summarized by the following points:

- A highly flexible and versatile industrial relevant R2R inkjet printing system was developed using equipments procured by Fujifilm Dimatix and Heraeus Noblelight GmbH.
- The QS-256/10 AAA class printheads having native resolution of 100 dpi were successfully implemented to achieve even higher resolution, i.e., >847 dpi but certain tuning was found to be necessary.
- By the implementation of the present print settings and equipments, it is possible to achieve line feature size of about 100 ± 25 μm and all other geometrical shapes.
- The IR technology could be classified as one of the best sintering tools for post-treating Ag nanoparticle inks, by which sheet resistance of below 0.5 Ω/□ could be obtained at a web speed of about 0.1 m/s.

ACKNOWLEDGMENT

The authors are grateful to their R&D partners, Mr. Jürgen Weber from Heraeus Noblelight GmbH, ImageXpert Inc. and FUJIFILM Dimatix, for their immense support by providing the equipment and their necessary technical information. We would also like to thank Department of Digital Printing and Imaging Technology, Technische Universität Chemnitz and Printed Functionalities, Fraunhofer ENAS for the printing and electrical characterization related facilities. Last but not least, the authors thank the important financial support given by the funding sources: EU funded project TDK4PE—GA number 287682, BMBF funded project PELWNC—FKZ 01DS17006, BMBF funded project EPOS—FKZ 03EK3529K, BMBF funded project leiTEX—FKZ 03ZZ0616G, BMWi ZIM funded project Yield Max—FKZ ZF4273103WO7, FhG funded internal project bioElektron (MAVO) – 600644 and FhG funded internal project Go Beyond 4.0 (leitProjekt) – 600776.

REFERENCES

1 E. Sowade, M. Polomoshnov, and R. Baumann, "The design challenge in printing devices and circuits: Influence of the orientation of print patterns in inkjet-printed electronics," Org. Electron. **37**, 428–438 (2016).

2 J. Niittynen, R. Abbel, M. Mäntysalo, J. Perelaer, U. S. Schubert, and D. Lupo, "Alternative sintering methods compared to conventional thermal sintering for inkjet printed silver nanoparticle ink," Thin Solid Films **556**, 452–459 (2014).

3 K-H Shin, H. A. D. Nguyen, J. Park, D. Shin, and D. Lee, "Roll-to-roll gravure printing of thick-film silver electrode micropatterns for flexible printed circuit board," J. Coat. Technol. Res. **14**, 95–106 (2017).

4 S. Alem, N. Graddage, J. Lu, T. Kololuoma, R. Movileanu, and Y. Tao, "Flexographic printing of polycarbazole-based inverted solar cells," J. Org. Electron. **52**, 146–152 (2018).

5 F. D. Giacomo, S. Shanmugam, H. Fledderus, B. J. Bruijnaers, W. J. H. Verhees, M. S. Dorenkamper, S. C. Veenstra, W. Qiu, R. Gehlhaar, T. Merckx, T. Aernouts, R. Andriessen, and Y. Galagan, "Up-scalable sheet-to-sheet production of high efficiency perovskite module and solar cells on 6-in. substrate using slot die coating," Sol. Energy Mater. Sol. Cells **181**, 53–59 (2018).

6 A. Amri, R. Rinaldi, and Khairat, "Synthesis of fluorinated tin oxide (FTO) using sustainable precursors and additions of graphene with spray coating deposition methods for transparent conductive material applications," Appl. Sci. Technol. **1**, 174–183 (2017).

7 K. Hayasaka, H. Matsui, Y. Takeda, R. Shiwaku, Y. Tanaka, T. Shiba, D. Kumaki, and S. Tokito, "Compact Organic Complementary D-Type Flip-Flop Circuits Fabricated with Inkjet Printing," Adv. Electron. Mater. **3**, 1700208 (2017).

8 S. Magdassi and A. Kamyshny, "Nanomaterials for 2D and 3D printing," *Chapter 4: Reactive Inkjet Printing as a Tool for in situ Synthesis of Self-Assembled Nanoparticles* (Wiley-VCH Verlag GmbH & Co. KGaA, Weinheim, Germany, 2017).

9 H. Kang, R. Kitsomboonloha, J. Jang, and V. Subramanian, "High-performance printed transistors realized using femtoliter gravure-printed sub-10 μm metallic nanoparticle patterns and highly uniform polymer dielectric and semiconductor layers," Adv. Mater. **24**, 3065–3069 (2012).

10 R. Zichner and R. Baumann, "Roll-to-roll screen printed radio frequency identification transponder antennas for vehicle tracking systems," Japan. J. Appl. Phys. **52**, 05DC24(1-4) (2013).

11 H. Kipphan, *Handbook of Print Media* (Springer, 2001).

12 Z. Werner, *Handbook of Industrial Inkjet Printing: A Full System Approach* (Wiley-VCH Verlag GmbH & Co. KGaA, Weinheim, Germany, 2017).

13 https://www.agfagraphics.com/global/en/product-finder/jeti-titan-s-hs.html.(Agfa).

14 https://www.kodak.com/DE/de/print/products/printers_presses/default.htm (Kodak).

15 http://www8.hp.com/de/de/commercial-printers/web-presses/T400-color-HD-series.html (HP).

16 E. Sowade, F. Göthel, R. Zichner, and R. R. Baumann, "Inkjet printing of UHF antennas on corrugated cardboards for packaging applications," Appl. Surf. Sci. **332**, 500–506 (2015).

17 H. F. Castro, E. Sowade, J. G. Rocha, P. Alpuim, S. Lanceros-Méndez, and R. R. Baumann, "All-inkjet-printed bottom-gate thin-film transistors using UV curable dielectric for well-defined source-drain electrodes," J. Electron. Mater. **43**, 2631–2636 (2014).

18 E. Sowade, E. Ramon, K. Y. Mitra, C. Martínez-Domingo, M. Pedró, J. Pallarès, F. Loffredo, F. Villani, H. L. Gomes, L. Terés, and R. R. Baumann, "All-inkjet-printed thin-film transistors: manufacturing process reliability by root cause analysis," Sci. Rep. **6**, 33490(1-15) (2016).

19 K. Y. Mitra, M. Polomoshnov, C. Martínez-Domingo, D. Mitra, E. Ramon, and R. R. Baumann, "Fully inkjet-printed thin-film transistor array manufactured on paper substrate for cheap electronic applications," Adv. Electron. Mater. **3**, 1700275(1-9) (2017).

20 S. Chung, S. Kim, S-K Kwon, C. Lee, and Y. Hong, "All-inkjet-printed organic thin-film transistor inverter on flexible plastic substrate," IEEE Electron Device Lett. **32**, 1134–1136 (2011).

21 D. Mitra, K. Y. Mitra, V. Dzhagan, N. Pillai, D. R. T. Zahn, and R. R. Baumann, "Work Function and conductivity of inkjet-printed silver layers: Effect of inks and post-treatments," J. Electron. Mater. **47**, 2135–2142 (2018).

22 J. Niittynen, E. Sowade, H. Kang, R. R. Baumann, and M. Mäntysalo, "Comparison of laser and intense pulsed light sintering (IPL) for inkjet-printed copper nanoparticle layers," Sci. Rep. **5**, 8832(1-10) (2015).

23 J. Perelaer, R. Jani, M. Grouchko, A. Kamyshny, S. Magdassi, and U. S. Schubert, "Plasma and microwave flash sintering of a tailored silver nanoparticle ink, yielding 60% bulk conductivity on cost-effective polymer foils," Adv. Mater. **24**, 3993–3998 (2012).

24 D. Mitra and R. R. Baumann, "Conductivity and microstructure of inkjet printed nanoparticle silver layers processed with intense pulsed light (IPL) sintering on various polymeric substrates," *Proc. IS&T Printing for Fabrication 2017 (NIP33) Int'l. Conf. on Digital Printing Technologies* (IS&T, Springfield, VA, 2017), pp. 92–96.

25 E. Sowade, H. Kang, K. Y. Mitra, O. J. Weiß, J. Weber, and R. R. Baumann, "Roll-to-roll infrared (IR) drying and sintering of an inkjet-printed silver nanoparticle ink within 1 s," J. Mater. Chem. C **3**, 11815–11826 (2015).

26 K. Y. Mitra, D. Weise, M. Hartwig, S. Kapadia, and R. R. Baumann, "Time-efficient curing of printed dielectrics via infra-red suitable to S2S and R2R manufacturing platforms for electronic devices," IEEE Trans. Electron Devices **63**, 2777–2784 (2016).

27 K. Y. Mitra, D. Weise, M. Hartwig, and R. R. Baumann, "Infra-red curing methodology for Roll-to-Roll (R2R) manufacturing of conductive electrodes through inkjet technology applicable for devices in the field of flexible electronics," *MRS Proceedings* (2015), Vol. 1791, p. 16.

28 E. Sowade, K. Y. Mitra, E. Ramon, C. Domingo, F. Villani, F. Loffredo, H. L. Gomes, and R. R. Baumann, "Up-scaling of the manufacturing of all-inkjet-printed organic thin-film transistors: Device performance and manufacturing yield of transistor arrays," Org. Electron. **30**, 237–246 (2016).

29 K. Y. Mitra, E. Sowade, C. Domingo, E. Ramon, J. Carrabina, H. L. Gomes, and R. R. Baumann, "Potential up-scaling of inkjet-printed devices for logical circuits in flexible electronics," *AIP Conference Proceeding* (2015), Vol. 1646, p. 106114.

30 R. Abbel, P. Teunissen, E. Rubingh, T. van Lammeren, R. Cauchois, M. Everaars, J. Valeton, S. van de Geijn, and P. Groen, "Industrial-scale inkjet printed electronics manufacturing-production up-scaling from concept tools to a roll-to-roll pilot line," Translational Mater. Res. **1**, 015002 (2014).

31 http://www.fujifilmusa.com/products/industrial_inkjet_printheads/print-products/product-dev-tools/mercury/index.html (Mercury Development Kit from FUJIFILM Dimatix) .

[32] http://www.fujifilmusa.com/products/industrial_inkjet_printheads/print-products/printheads/high-performance/sapphire-qs-256-10-aaa/index.html (Sapphire QS-256-10 AAA from FUJIFILM Dimatix).

[33] A. A. Khalate, X. Bombois, G. Scorletti, R. Babuška, S. Koekebakker, and W. de Zeeuw, "A Waveform Design Method for a Piezo Inkjet Printhead Based on Robust Feedforward Control," J. Microelectromech. Syst. **21**, 1365–1374 (2012).

[34] https://jetxpert.com/products/jetxpert/ (JetXpert from ImageXpert Inc.).

[35] S. D. Hoath, *Fundamentals of Inkjet Printing: The Science of Inkjet and Droplets*, Chapter 9: Coalescence and line formation (Wiley-VCH Verlag GmbH & Co. KGaA, Weinheim, Germany, 2016).

[36] P. C. Duineveld, "The stability of ink-jet printed lines of liquid with zero receding contact angle on a homogenous substrate," J. Fluid Mech. **477**, 175–200 (2003).

[37] T. H. J. van Osch, J. Perelaer, A. W. M. de Laat, and U. S. Schubert, "Inkjet printing of narrow conductive tracks on untreated polymeric substrates," J. Adv. Mater. **20**, 343–345 (2008).